PCCP

Physical Chemistry Chemical Physics

Accepted Manuscript

This article can be cited before page numbers have been issued, to do this please use: S. Góbi, B. Keresztes, A. Schneiker and G. Tarczay, *Phys. Chem. Chem. Phys.*, 2024, DOI: 10.1039/D4CP02400A.

View Article Online
DOI: 10.1039/D4CP02400A

PCCP

ARTICLE TYPE

Cite this: DOI: 00.0000/xxxxxxxxxx

Hydrogen-atom-assisted processes on thioacetamide in *para*-H_2 matrix – Formation of thiol tautomers†

Sándor Góbi,*[a,b] Barbara Keresztes,[a,c], Anita Schneiker[a,c] and György Tarczay[a,b,d]

Received Date
Accepted Date

DOI: 00.0000/xxxxxxxxxx

TA has been isolated in low-temperature *para*-H_2 matrices and it has been exposed to H atoms. In accordance with previous experimental results, TA exclusively exists in its more stable thione tautomeric form in the freshly deposited matrix. However, upon H atom generation, the bands belonging to the precursor start decreasing with the simultaneous appearance of new bands. By comparing the position of these new peaks with earlier results obtained in *para*-H_2, they can be undoubtedly attributed to the presence of the higher-energy thiol tautomeric forms of TA. No other products could be observed, except for NH_3. Quantum-chemical computations have been invoked to understand the mechanism behind the observed thione–thiol tautomerization assisted by H atoms. Accordingly, the tautomerization starts with a barrierless H-atom addition on the S atom of the thione resulting in the formation of the intermediate 1-amino-1-mercapto-ethyl radical ($H_3C–\dot{C}(–SH)–NH_2$), which has been detected tentatively for the first time. The second step is a barrierless H-atom induced H-abstraction from the $–NH_2$ moiety of the $H_3C–\dot{C}(–SH)–NH_2$ radical. A comprehensive mechanism for tautomerization is proposed based on the experimental and theoretical results. Although earlier studies showed the possibility of TA thione–thiol tautomerization in cryogenic matrices achieved by energetic UV irradiation, the present study points out that this can also take place through a barrierless pathway by simply exposing the TA molecules to H atoms. As such, this is the first evidence for the occurrence of such a reaction in a matrix-isolated environment. The current results also help us better understand the mystery behind thione–thiol tautomerization in a low-temperature matrix environment.

1 Introduction

Thioacetamide (TA) has been extensively studied by the matrix-isolation (MI) technique in the past several years. Originally, the freshly deposited matrix contains the more stable thione tautomeric form (Figure 1, *left*) exclusively. However, its tautomerization into the less stable thiol form (Figure 1, *right*) can be induced by simple energetic radiation, namely, exposing the sample to longer wavelength (> 240 nm) UV photons.[1] Later, the present authors pointed out that the higher-energy thiol rotamers spontaneously convert into each other *via* H-atom tunneling.[2] Moreover, this interconversion can be selectively facilitated by utilizing near-IR (NIR) laser light by exciting their NH stretching overtone (2ν[NH]).[3] Furthermore, UV radiation below 240 nm induces tautomerization along with decomposition leading to the formation of a plethora of irradiation products.[4] Hydrogen (or H)-atom reactions can also be conducted in cryogenic matrices (mostly in *para*-H_2 and in Xe), which proved to be a powerful tool, for instance, to simulate similar processes in the interstellar medium (*e.g.*, Refs 5,6). Although matrix-isolated samples may not perfectly simulate real-world systems, they have a few advantages. First, the interaction of the host material with the guest molecules is negligible resulting in a significant decrease in the spectral bandwidths compared to those obtained in the condensed phase. The better spectral resolution means fewer overlapping bands and better agreement with the spectra predicted by theory, therefore easier interpretation. Second, the migration of primary products (such as radicals) is inhibited in rigid matrices, allowing for their direct observation thus the easier understanding of the reaction mechanism.

Besides the more conventional host materials, like frozen noble gases, the more exotic *para*-H_2 enables the generation of H atoms. This solid quantum material has a few unique features compared to the more traditional hosts.[7,8] One of them is the

[a] *Laboratory of Molecular Spectroscopy, Institute of Chemistry, ELTE Eötvös Loránd University, PO Box 32, H-1518 Budapest, Hungary; E-mail: sandor.gobi@ttk.elte.hu*
[b] *MTA-ELTE Lendület Laboratory Astrochemistry Research Group, Institute of Chemistry, ELTE Eötvös Loránd University, PO Box 32, H-1518 Budapest, Hungary*
[c] *Hevesy György PhD School of Chemistry, Institute of Chemistry, ELTE Eötvös Loránd University, PO Box 32, H-1518 Budapest, Hungary*
[d] *Centre for Astrophysics and Space Science, ELTE Eötvös Loránd University, PO Box 32, H-1518 Budapest, Hungary*

† Electronic Supplementary Information (ESI) available: [details of any supplementary information available should be included here]. See DOI: 10.1039/cXCP00000x/

View Article Online
DOI: 10.1039/D4CP02400A

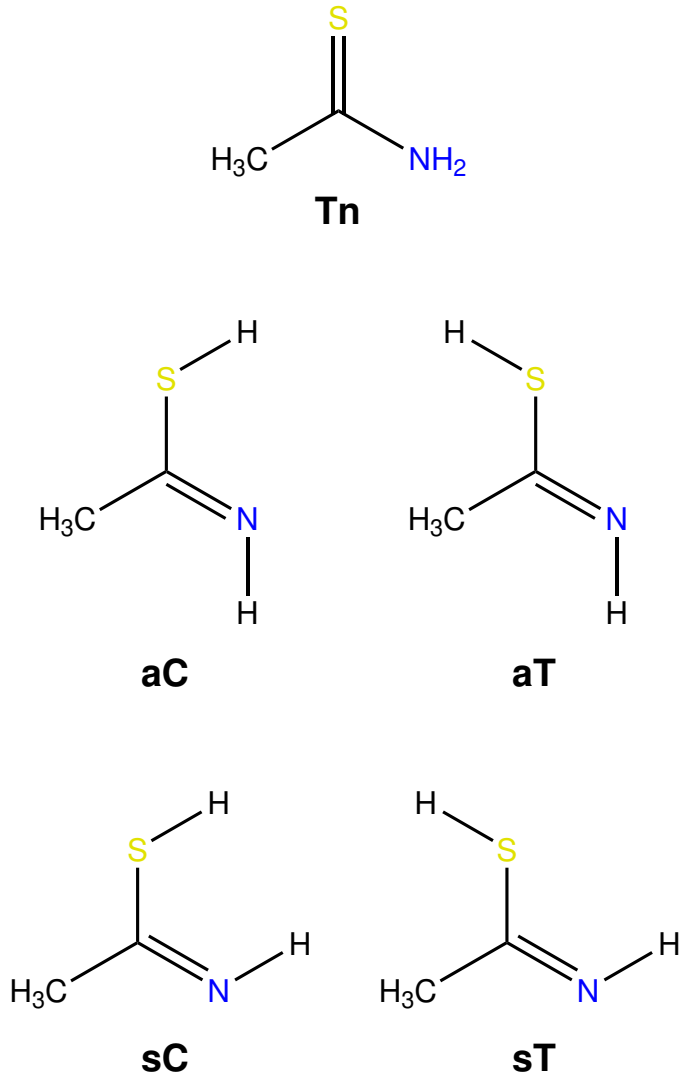

Fig. 1 The thione (Tn) and the four thiol tautomers of TA.

so-called quantum diffusion of H atoms throughout the matrix, enabling the study of H-atom reactions. Moreover, there is even less interaction with sample molecules resulting in peaks that are even sharper in the spectrum than in, *e.g.*, Ar. The diminishing cage effect also allows for the detection of radicals that would otherwise recombine.[4,9] Compared to noble gas hosts, higher H-atom tunneling rates were observed in *para*-H_2.[10] Accordingly, the question arises what processes could be observed when TA isolated in *para*-H_2 matrix is exposed to H atoms. It would be a reasonable assumption that part of the TA thione tautomers, exclusively prevailing in the unprocessed matrix, would undergo a tautomerization into the higher-energy thiol form. As such, this would be the first occasion of a thione–thiol tautomerization in the absence of a radiation field, by simply exposing the sample to H atoms.

2 Materials and Methods

The MI experiments were performed on the VIZSLA setup consisting of an ultrahigh-vacuum (UHV) compatible stainless steel chamber with a base pressure of 1×10^{-9} mbar when cooled.[11] The matrix host was *para*-H_2, which was prepared by converting *normal*-H_2 (Messer, 99.999%) on porous Fe(III) oxide (Sigma-Aldrich (St. Louis, MI, USA), hydrated, catalyst grade, 30–50 mesh) catalyst. The catalyst was filled into a stainless steel capillary wrapped around the 10 K cryostat (CH202, Sumitomo Heavy Industries Inc.) of the setup, which was cooled down to 13.9 K. The *para*-H_2 was collected in a 0.5 L glass flask on a gas mixing line, also connected to the simulation chamber through a high-purity copper tube 6 mm in diameter.

The matrix was prepared by co-depositing TA (Sigma-Aldrich, $>$ 99%) and *para*-H_2 on a gold-plated silver wafer serving as the substrate, attached to the cold finger of the 3 K cryostat of the setup (RDK-415D, Sumitomo Heavy Industries Inc.). The TA sample was at room temperature providing a sufficient vapor pressure for the deposition, which was done for 125 min through a Teflon tube 6 mm in diameter ending *ca*. 3 cm before the substrate. The *para*-H_2 was introduced into the main chamber *via* a stainless steel capillary array through a leak valve; the distance between the substrate and the end of the capillaries was approximately 3 cm as well. The inlet rate was kept at $\approx$ 0.8 mbar L min^{-1}. For the H-atom-reaction studies, the matrix had to be doped with molecular Cl_2, which was introduced using another leak valve and capillary array; the Cl_2 to *para*-H_2 ratio was roughly 1 : 500.

The H atoms were generated utilizing the two-step process developed by Raston *et al.*[12–16] According to this, the deposited matrix was first subjected to an LED irradation at 365 nm (M365L3 LED source, ThorLabs, *fwhm* $\approx$ 9 nm, equipped with an SM1U collimation adapter and a LEDD1B driver) for 31 + 30 minutes using a current of I = 0.15 and 0.25 A to induce the Cl_2 dissociation thus the generation of Cl atoms. Due to the already-mentioned diminished cage effect in *para*-H_2, the formed Cl atoms may rapidly diffuse away from each other thus reducing the likelihood of recombination. Subsequently, the 2217 nm (NIR) laser excitation of the $Q_1(1) + S_0(0)$ and $Q_1(0) + S_0(0)$ combination bands of the *para*-H_2 molecules allows for the Cl + *para*-H_2 reaction leading to the formation of H and HCl. This 2217 nm irradiation was conducted by applying an optical parametric oscillator (OPO, GWU / Spectra-Physics VersaScan MB 240, *fwhm* $\approx$ 5 cm^{-1}) equipped with a frequency-doubling unit (Spectra-Physics uvScan) pumped by a pulsed Nd:YAG laser (Spectra-Physics Quanta Ray Lab 150, $P \approx$ 1.9–2.0 W, λ = 355 nm, f = 10 Hz, pulse duration = 2–3 ns). The 2217 nm irradiation took 80 minutes, the utilized output power was P = 0.8–1.0 mJ. Then, this H atom generation was repeated by applying 30 min of 365 mn LED irradiation (I = 0.33 A) and 60 min of 2217 nm irradiation (P = 1.0–1.1 mJ). After the irradiations, the matrix was kept in the dark overnight, to let the remaining H atoms diffuse in the soft matrix and participate in addition and abstraction reactions. A blank experiment was also carried out, which was identical in every step except that it was done without Cl_2 in the matrix, the 365 nm LED irradiation took 45 minutes, and the 2217 nm NIR laser irradiation lasted 90 minutes.

Mid-IR (MIR) spectra were taken by a Bruker Invenio FT-IR spectrometer working in reflection–absorption mode utilizing a liquid N_2-cooled mid-band Mercury Cadmium Telluride (MCT)

View Article Online
DOI: 10.1039/D4CP02400A

detector in the spectral region of 4000–600 cm^{-1} at a resolution of 0.5 cm^{-1}. 32 scans were averaged in each minute during deposition and the 2217 nm laser irradiation. In the latter case, *i.e.*, during the NIR laser irradiation, a low-pass filter with a cutoff wavenumber of 3860 cm^{-1} was utilized to prevent the interference between the laser photons with the MCT detector. After the irradiation cycles, 128-scan spectra were saved every 30 minutes in the dark. MIR background spectra with as well as without the cutoff filter were collected just before the deposition at the same temperature and resolution as during the experiment averaging 256 scans. An NIR background spectrum averaging 128 scans was also collected before the experiment. Furthermore, one NIR sample spectrum of 32 scans was saved after deposition in order to determine the purity (in other words, the *ortho*-H_2 concentration) of the matrix along with its optical path length (which is necessitated to determine the mixing ratios of the matrix-isolated species). The implemented mixing ratio calculation is based on what is discussed in Ref. 7 and is detailed elsewhere.[4] NIR spectra were also collected after the 31 min of the first 365 nm irradiation (by interrupting it) and at the end of both the first and second 365 nm irradiation cycles to check for the presence of the forming Cl atoms in the matrix.

Quantum-chemical DFT computations were also performed utilizing the Gaussian 09 software (Rev. D01).[17] The geometry of the structure of the precursors and the identified H-atom-reaction products was optimized at the B3LYP/cc-pV(T+d)Z level of theory. Afterwards, harmonic and anharmonic vibrational frequencies and intensities of the minima structures as well as those of the transition states (TSs, if any) were computed at the same level of theory applying the vibrational perturbation theory (VPT2) for the anharmonic computations.[18,19]

3 Results and Discussion

3.1 H-atom reaction studies

The MIR spectrum of TA obtained in *para*-H_2 is in good agreement with previous experimental results;[4] that of the freshly deposited sample as well as the vibrational assignment of the matrix-isolated precursor molecule can be found in the Supporting Information (Figure S1 and Table S1). Upon generating H atoms, the appearance of new spectral bands can evidently be observed, as visualized in Figure 2. The position of these new peaks is in excellent agreement with those of the higher-energy thiol tautomeric form of TA when compared to the results of previous UV irradiation studies done in various cryogenic matrices.[1–4] The vibrational assignment of the thiol tautomers is summarized in Table 1; the same notation is used for the thiol rotamers as in our previous works.[2–4] The softer *para*-H_2 matrix allows for an uninhibited intra- or intermolecular rotation of the TA molecules, resulting in the fact that the bandwidths are notably larger than in Ar. This is in complete accordance with previous results,[4] which also makes the separation of the signals of the particular thiol rotamers pretty difficult in some cases. It should be noted that besides the evident formation of thiols, one more product could also be observed unambiguously in the irradiated spectrum. Ammonia, NH_3, can be identified through its symmetric bending

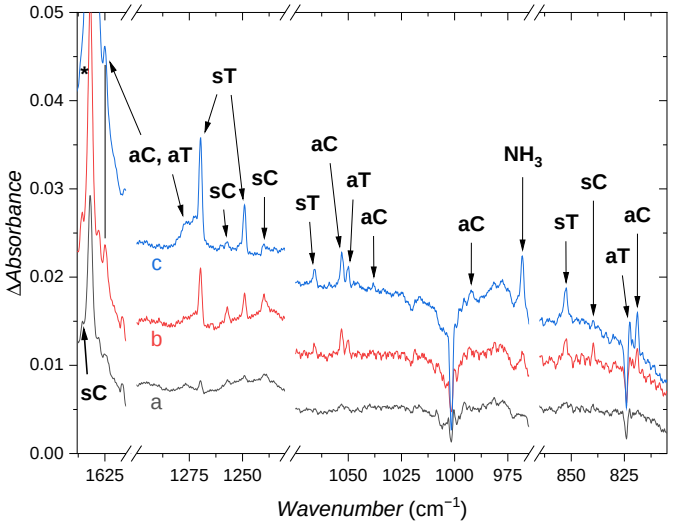

Fig. 2 Sections of the MIR difference spectra of TA in *para*-H_2 matrix after the first (a, dark grey trace) and second (b, red) H atom generations, as well as after keeping the sample in the dark (c, blue). The spectra are offset for clarity; the labels denote the various thiol rotamers as well as NH_3. The asterisk marks the forming *ortho*-H_2O band, which can always be observed upon H atom generation, whereas the black vertical line at the 1625 cm^{-1} helps in following the trend. The spectrum taken right after deposition serves as a reference.

($\beta_s[NH_3]$) vibrational mode with the maximum at 968.3 cm^{-1}.[20] It should be noted, however, that there is an intense complex band with the strongest one centered at around 2378 cm^{-1} (Figure S2 in the Supporting Information). A tentative assignment for this spectral feature will also be given.

3.2 Kinetics of the tautomerization

The assignment of the forming thiol absorption bands was also helped by plotting the temporal behavior. Based on the method used for *para*-H_2 matrices,[7] the full procedure is described in detail elsewhere.[4] Accordingly, the optical path could be determined to be 0.279 ± 0.007 mm in the freshly deposited matrix. Also in line with previous findings, the harmonic computed infrared intensities were used instead of the anharmonic ones, due to the questionable reliability of the latter, especially regarding low-frequency vibrations.[9] To be able to estimate the uncertainty of the data points on the kinetic plot, multiple peaks were considered, wherever it was possible. For the TA thione precursor, three peaks were taken into account, which are the ones at 3528.4, 3411.1, and 1373.4 cm^{-1} with the computed harmonic IR intensities of 35.7, 41.2, and 48.1 km mol^{-1}, respectively (please refer to Table S1 in the Supporting Information for the band assignment). These bands are strong enough but do not overlap extensively, allowing for the proper determination of the mixing ratio with relatively low uncertainties. As far as thiols are concerned, the mixing ratio of the **aC** rotamer could be determined using its 1052.9 cm^{-1} (61.6 km mol^{-1}) and 819.3 cm^{-1} (51.8 km mol^{-1}) bands. The **aT** rotamer displayed two peaks that could be used, the ones at 1050.3 cm^{-1} (76.1 km mol^{-1}) and 822.2 cm^{-1} (56.9 km mol^{-1}). The same applies to the **sC** thiol, the two considered absorption features can be found at

View Article Online
DOI: 10.1039/D4CP02400A

Table 1 Vibrational absorption features of the thiol tautomers after exposing TA to H-atoms in *para*-H_2 matrix; as well as the comparison with literature data.

Vibrational mode[a]	*para*-H_2[b] $\tilde{\nu}$[d]	Ar[c] $\tilde{\nu}$[d]	Ar[c] I[e]
sC ν[C=N]	1636.1sh	1632	130
aT ν[C=N]	1624.8sh	1621	145
aC ν[C=N]		1620sh	65
aT β'_{as}[CH_3]	1442.6b	1441	20
aC β'_{as}[CH_3]		1440	26
aC β''_{as}[CH_3]	1435.2b	1434	36
aT β''_{as}[CH_3]		1433	29
aC β[NH]	1273.1b	1272	41
aT 2ν[NH]		1270	10
sT β[NH]	1269.9	1267	244
sC β[NH]	1257.4	1254	107
sT 2ν[C–S]	1249.1	1244	54
sC 2ν[C–S]	1240.0	1236	74
sT ρ′[CH_3]	1065.9	1063	29
aC ρ′[CH_3]	1052.9	1050	77
aT ρ′[CH_3]	1050.3	1047	38
aC ρ″[CH_3]	1038.4	1036	15
aC ν[C–C]	992.8	991	38
sT γ[NH]	852.9	849	108
sC γ[NH]	840.2	836	64
aT γ[NH]	822.2	818	65
aC γ[NH]	819.3	816	83
aT ν[C–S]	*643.6*	640	43
sT ν[C–S]	*628.9*	623	32

[a] Vibrational assignment based on Ref. 3; ν:stretching, β: in-plane bending, ρ: rocking, γ: out-of-plane bending, s: symmetric, as: antisymmetric vibrations.
[b] This work.
[c] Ar-matrix data taken from Ref. 3.
[d] in cm^{-1}, sh: shoulder, b: broad. Values in italic could not be observed in the present study, only by Ref. 4.
[e] Normalized experimental band areas. The values were obtained by multiplying the integrated area of a band in the experimental infrared spectrum by the sum of the theoretical infrared intensities then dividing by the sum of the experimental band areas.

1257.4 cm^{-1} (245 km mol^{-1}) and 840.2 cm^{-1} (59.8 km mol^{-1}), respectively. The fourth rotamer, **sT**, has an exceptionally strong signal with the maximum at 1269.9 cm^{-1} (240 km mol^{-1}) that could be used to prepare the kinetic plot.

According to Figure 3, all four thiol forms appear under the 2217 nm NIR laser irradiation, and their concentration continuously increases during the process, whereas that of the originally exclusive thione form decreases. The **sC** isomer is well-known to spontaneously convert into the more stable **sT** form in cryogenic matrices through H atom tunneling.[3] This process can be recognized in the overnight part of the kinetic curve, when the sample is kept in the dark. As for the other two isomers, **aC** and **aT**, both of them increase gradually over time. As far as the other two species, NH_3 and the unassigned 2378 cm^{-1} band are concerned, the former one also shows a monotonic growth similar to those of the thiols, whereas the other grows only during the

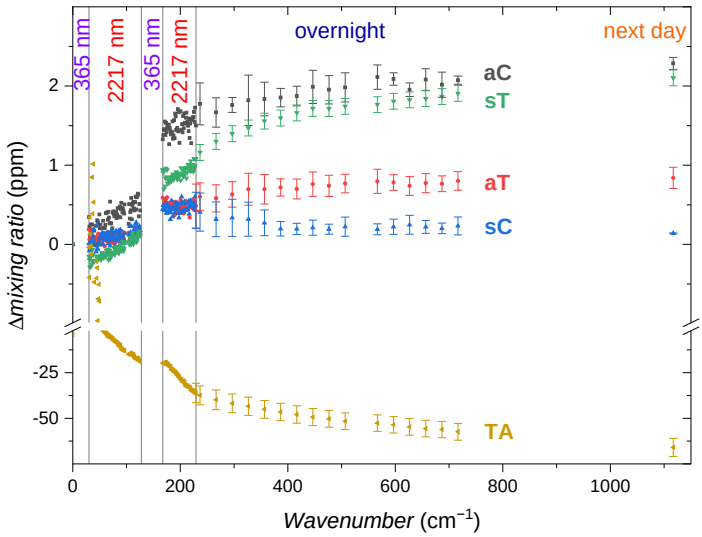

Fig. 3 Kinetic curves of TA thione and thiol tautomers during and after H atom generation; the error bars during the irradiation part are omitted for clarity.

2217 nm irradiation and overnight (and is completely bleached during the second 365 nm irradiation, Figure S3 in the Supporting Information).

3.3 Computational results of the H-atom processes

3.3.1 TA thione tautomer

The Supporting Information contains all the optimized geometries of the minima (Tables S2–S28) and those of the found transition states (TSs, Tables S29–S108) along with the barrier heights of the processes (Tables S109–S135). When the thione tautomeric form of TA (H_3C–C(=S)–NH_2) is exposed to H atoms generated in the cryogenic *para*-H_2 matrix, the H atoms may initially attack four sites on the TA molecule: at the methyl (–CH_3) or the amino (–NH_2) groups for a bimolecular homolytic substitution (S_H2) or at the C or the S atoms resulting in H-atom addition. Kobayashi *et al.*[21] showed that the last process is barrierless, in contrast to the case when the addition occurs on the C atom (19.3 kJ mol^{-1}); the S_H2 process involving either the –CH_3 or –NH_2 groups were not considered by those authors but can be expected to have large barriers nonetheless. And indeed, the barrier of the H-atom addition onto the C atom is computed to be 17.4 kJ mol^{-1} and the same process on the S atom is barrierless, in accordance with the above-mentioned literature results. Note that all computational results presented here are zero-point vibrational energy (ZPVE) corrected values. The S_H2 reactions of the –CH_3 or –NH_2 groups, resulting in the elimination of either methane (CH_4) or ammonia (NH_3) have barrier heights of 124 kJ mol^{-1} and 30.2 kJ mol^{-1}, respectively. One can expect that only the processes with (near)-zero barriers may take place, therefore all H-atom-addition processes can be safely ruled out, except for the one that occurs on the S atom. Briefly, only the formation of the 1-amino-1-mercapto-ethyl radical (H_3C–Ċ(–SH)–NH_2), three conformers) based on the orientation of the –SH and –NH_2 groups, respectively. It is also worth noting that H-atom

View Article Online
DOI: 10.1039/D4CP02400A

abstraction induced by the incoming H atom can also occur. In this case, the abstraction can happen on either the $–CH_3$ group or the $–NH_2$ group of the TA thione. In both cases, the theory found non-negligible barriers with heights of 11.7 kJ mol^{-1} and 22.3 kJ mol^{-1}. One should bear in mind that it is expected that processes with several tens of kJ mol^{-1} barrier cannot occur by tunneling on the laboratory timescale. Even if they are allowed to take place, the rate of the numerous competitive barrierless processes is expected to be significantly higher, rendering the pathways with reaction barriers less significant. Lastly, even if these processes occur, the thione form is quickly regenerated after a rapid, barrierless H-atom addition on the radical centers of the H-abstraction products. In other words, the H-abstraction of thione is not likely to be directly observed upon H-atom generation. Based on the above considerations, only the products of the barrierless processes are taken into account in the next subsections of this work.

3.3.2 1-amino-1-mercapto-ethyl radical ($H_3C–\dot{C}(–SH)–NH_2$)

The intermediate $H_3C–\dot{C}(–SH)–NH_2$ radical can be assumed to be sensitive to the presence of H atoms, *i.e.*, it may readily take part in further H-atom processes. The anticipated reaction channels can both be H-atom addition and abstraction. In the former case, namely, when the exposure to H atoms results in H-addition, the target can be either the S or the central C atom. One would assume that, similarly to what could be experienced for the precursor thione TA form, the S_H2 reactions of the terminal $–NH_2$ and $–CH_3$ groups have high barriers. Interestingly, all structures resulted in barrierless H-abstraction processes as per the computations (see below) thus no TSs could be determined for this kind of reaction of these two groups. In contrast, the H-addition on the S and the C atoms are both found to be barrierless by theory, with the former one resulting in the elimination of H_2S and the latter one yielding 1-amino ethanethiol ($H_3C–CH(–SH)–NH_2$, nine conformers). As far as the H-abstraction processes are concerned, they may occur on the $–CH_3$, the $–NH_2$, and on the –SH groups, leading to the formation of 1-amino-ethenethiol ($H_2C=C(–SH)–NH_2$, three conformers depending on the relative orientation of the –SH and $–NH_2$ groups), the four TA thiol rotamers ($H_3C–C(–SH)=NH$), and the initial TA thione form. Interestingly, all three processes are barrierless according to the quantum-chemical computations. Out of these three molecules, $H_2C=C(–SH)–NH_2$ cannot be observed in contrast to thiols, which are the most abundant product molecules of the TA molecules exposed to H atoms. The lack of $H_2C=C(–SH)–NH_2$ in the spectrum can be simply explained by its rapid conversion back to the $H_3C–\dot{C}(–SH)–NH_2$ radical *via* a barrierless H-atom addition on the $=CH_2$ group. For the sake of completeness, one should mention its other reactions involving H atoms, such as the elimination of H_2S after a barrierless H-atom addition on the –SH group. In contrast, the computations found barrier heights of 6.9–17.1 kJ mol^{-1} for the H addition on the C atom, and considerable ones that result in the elimination of the small NH_3 molecule (S_H2 process on the $–NH_2$ moiety, 38.4–42.1 kJ mol^{-1}). The $H_2C=C(–SH)–NH_2$ molecule may participate in H-atom-induced H-abstraction processes, too. And, as expected, the abstraction from the –SH group is barrierless, whereas the same process on the $=CH_2$ or $–NH_2$ groups are hindered (with barrier heights of 54.0 and $\approx$ 7 kJ mol^{-1}, respectively).

3.3.3 1-amino-ethanethiol ($H_3C–CH(–SH)–NH_2$)

The same holds true for $H_3C–CH(–SH)–NH_2$, whose back conversion to $H_3C–\dot{C}(–SH)–NH_2$ through H-atom abstraction is predicted by the computations to be barrierless for three conformers (for the other six, the process is found to be kinetically unfavored by 1.5–4.2 kJ mol^{-1}, which are comparable to the accuracy of the theoretical method used). This is in contrast to what was found for the H-atom abstraction from the $–CH_3$ or the $–NH_2$ groups, which both have barriers of 7.7–30.9 kJ mol^{-1} and 9.8–24.1 kJ mol^{-1}, respectively. One more H-abstraction that can occur on the $H_3C–CH(–SH)–NH_2$ is another barrierless one that involves the –SH group, ultimately yielding the 1-amino-ethylthiyl radical ($H_3C–CH(–\dot{S})–NH_2$, 3 chiral rotamers depending on the orientation of the $–NH_2$ moiety). However, no traces of $H_3C–CH(–\dot{S})–NH_2$ were detected in the IR spectrum. This is most likely due to the fact that the H-atom-addition reaction on its S atom is also barrierless, thus quickly regenerating the stable $H_3C–CH(–SH)–NH_2$ molecule. Another possibility is the barrierless H-atom-induced H-atom abstraction from the chiral C atom $H_3C–CH(–\dot{S})–NH_2$ leading to the regeneration of the thione precursor. For the sake of completeness, it should be noted that the theory also suggests that the barrierless H-abstraction may work on the $–CH_3$ as well as on the $–NH_2$ groups of the $H_3C–CH(–\dot{S})–NH_2$ radical eventually yielding the cyclic $[(H_2)CSC(H)]–NH_2$ and the $H_3C–[(H)CSN(H)]$ molecules, respectively. However, no spectral evidence was found for their existence in the matrix after H-atom generation. The S_H2 reactions were also predicted to occur without any barrier, resulting in CH_4 or NH_3 elimination, when an H atom attacks the $–CH_3$ or the $–NH_2$ groups, respectively.

Other reactions of $H_3C–CH(–SH)–NH_2$ may involve further H-atom addition occurring on the S atom of the –SH group, thus resulting in the elimination of H_2S, which was found to have no barrier. The S_H2 reaction involving the N atom as well as on the C atom of $–CH_3$, which would otherwise lead to the elimination of either NH_3 or CH_4, both have significant barriers (39-58 kJ mol^{-1} and 110-120 kJ mol^{-1}, respectively). Moreover, the theory found the former process to be endothermic.

3.3.4 TA thiol tautomer and the $H_3C–C(–\dot{S})–NH$ radical

The forming thiols were also predicted not to be completely stable against H atoms generated in the matrix. Among the H-addition processes, the one involving the –SH group is barrierless and yields H_2S, in line with the former findings. In contrast, the S_H2 process related to the $–CH_3$ group or the addition on the central C atom (which would generate CH_4 or the $H_3C–CH(–SH)–\dot{N}H$ radical) have barrier heights that prevents them to take place (119–126 kJ mol^{-1} and 30.9–31.7 kJ mol^{-1}, respectively). The addition on the =NH moiety is an intermediate in this sense, with a computed barrier height of 2.1–3.2 kJ mol^{-1}, which is within the accuracy of the computation, therefore its occurrence cannot be ruled out, regenerating the $H_3C–\dot{C}(–SH)–NH_2$ radical. As for the H-atom-abstraction reactions, the H-atom-induced H-

View Article Online
DOI: 10.1039/D4CP02400A

atom abstraction from the S atom is also barrierless, leading to the formation of the $H_3C–C(–\dot{S})=NH$ radical (2 rotamers). Similarly to what can be experienced in the H-atom-addition process, the H-abstraction from the –NH group also has a negligible barrier (from barrierless to 2.4 kJ mol^{-1} depending on the thiol rotamer) yielding the isomer of $H_3C–C(–\dot{S})–NH$, namely $H_3C–C(–SH)=\dot{N}$. In contrast, the H-atom abstraction occurring on the $–CH_3$ functional group of the thiols is kinetically unfavored (with barrier heights of 17.3–17.9 kJ mol^{-1}).

For the sake of completeness, one should also mention the reactions of the C_2H_4NS isomers, even though there is no proof for their presence in the matrix after H-atom generation. The formed $H_3C–C(–\dot{S})–NH$ radical can also participate in H-atom reactions, which are all predicted to be barrierless. This is not unexpected for the H-addition processes on either the S or the N atoms, regenerating either the TA thiol rotamers or the thione precursor, respectively. Besides, the S_H2 process on the $–CH_3$ group involves the formation of the stable molecules isothiocyanic acid (HNCS) and CH_4 but no TS could be identified by the computations. Nevertheless, no evidence for HNCS formation was found in the sample exposed to H atoms. The unhindered H-abstraction from the –NH group of $H_3C–C(–\dot{S})–NH$ yields the strained cyclic $H_3C–[CSN]$ molecule, in line with the findings for the thiol rotamers. Less expected is the kinetically allowed H-abstraction from the $–CH_3$ moiety resulting in the formation of another cyclic compound, $H_2[CSC]=NH$. As for the other C_2H_4NS isomer, $H_3C–C(–SH)=\dot{N}$, the barrierless H-atom addition on the –SH group results in H_2S elimination and the formation of methyl cyanide ($H_3C–CN$), as expected. No spectroscopic evidence was found for the existence of $H_3C–CN$ in the processed matrix, however. Similarly, the kinetically favored addition on the N atom converts the molecule back to thiols. The S_H2 process involving the $–CH_3$ moiety involves the formation of CH_4 and HSCN, however, no TSs could be determined by the computations. The H-atom abstraction may only occur on the $–CH_3$ group according to the computations, leading to the formation of another three-membered cyclic structrure, $H_2[CNC]–SH$. In contrast, the abstraction from the –SH group gave no meaningful results. Finally, it is worth noting that the theoretical results suggest that almost all H-atom reaction channels are basically unhindered in the case of the radicals, independently whether they are C_2H_4NS or C_2H_6NS isomers.

3.4 Proposed mechanism for the thione–thiol tautomerization

Based on the computational results, one can compile a reaction mechanism scheme of the H-atom processes occurring in the *para*-H_2 matrix containing TA thione monomers (Figure 4). The thione precursor form rapidly evolves into the S-hydrogenated form $H_3C–\dot{C}(–SH)–NH_2$, which latter becomes the centerpiece of the reaction scheme. The most important pathway according to the experimental results is the one leading to the thiol tautomeric form, but the one with the $H_3C–CH(–SH)–NH_2$ is also expected to be important. Other, less important reaction channels may be the dehydrogenation of $H_3C–CH(–SH)–NH_2$ back to thiones through the $H_3C–CH(–\dot{S})–NH_2$ intermediate, the conversion of $H_3C–\dot{C}(–$

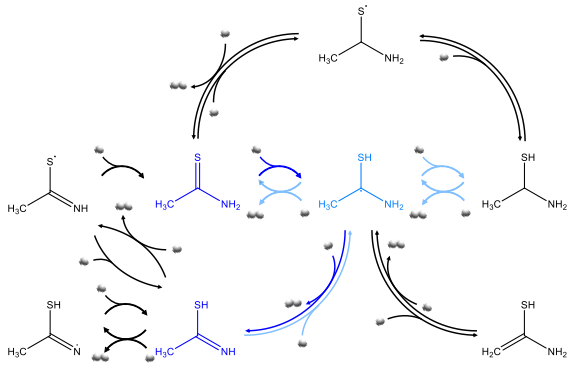

Fig. 4 Proposed reaction scheme of TA decomposition upon H-atom generation; the scheme contains only the most important (barrierless) reaction channels, excluding the ones involving the elimination of H_2S, for the sake of clarity. Molecules in dark blue were experimentally observed, whereas the one in light blue were identified tentatively; arrows in dark blue show the most possible reaction pathways and light blue arrows show processes that may be also important although there is no experimental evidence for their occurrence.

$SH)–NH_2$ into $H_2C=C(–SH)–NH_2$, and the tautomerization of thiols back to thiones *via* the $H_3C–C(–\dot{S})=NH$ radical. Consequently, these back and forth hydrogenation / dehydrogenation channels (along with H atom recombination into H_2) may efficiently consume the overall H atom budget and may contribute to the eventually observed low concentration of H-atom-reaction products including the undoubtedly observed one, namely, the thiol tautomeric forms. In contrast, it is rather difficult to explain the presence and formation of the other unambiguous product, NH_3, based on the computational results since they predict the NH_3 formation upon the S_H2 process to be kinetically hindered. Nevertheless, the impact of Cl atoms or HCl as well as tunneling processes on their formation cannot be ruled out.

One should also discuss the bearer of the hitherto unassigned 2378 cm^{-1} band, which may be tentatively attributed to the $H_3C–\dot{C}(–SH)–NH_2$ radical. The assignment can be primarily based on the kinetic behavior of this band, namely, that it grows significantly during the H-atom generation (2217 nm irradiation), during which there are plenty of H atoms in the matrix. Radicals are usually photo-labile, which may explain why this band disappears during the second 365 nm UV irradiation. Lastly, the gradually increasing growth rate of the mixing ratio in the kinetic curve during the night implies that as the H atom concentration decreases, the chance for a second H-atom reaction (*e.g.*, thiol formation) diminishes, allowing for the radical to accumulate. The computational results also corroborate the vibrational assignment; the ν[S–H] vibrational mode of some $H_3C–\dot{C}(–SH)–NH_2$ rotamers has an anomalously low predicted anharmonic vibrational frequency of approximately 2310 cm^{-1} and an unexpectedly high theoretical intensity of $\approx$ 100 km mol^{-1}. In other words, this particular vibrational mode of this radical is greatly shifted towards smaller frequencies and significantly stronger than most ν[S–H] vibrations of other molecules. Unfortunately, the other vibrational modes of this radical are computed either to be too weak or expected to overlap with the bands of the precursor (or thiols) ren-

View Article Online
DOI: 10.1039/D4CP02400A

Table 2 Change in mixing ratios (in ppm) of the TA thione precursor and the TA thiol products right after H atom generation and after waiting ≈15 h in the dark.

Species	Δmixing ratio	
	after H atom generation	next day
Precursor	-37 ± 5	-66 ± 5
aC	1.8 ± 0.3	2.3 ± 0.1
aT	0.6 ± 0.2	0.8 ± 0.1
sC	0.4 ± 0.2	0.1 ± 0.1
sT	1.2 ± 0.1	2.1 ± 0.1
NH_3	0.3 ± 0.1	1.2 ± 0.1
C balance[a]	$(11 \pm 4)\%$	$(8 \pm 1)\%$
S balance	$(11 \pm 4)\%$	$(8 \pm 1)\%$
N balance[a]	$(12 \pm 3)\%$	$(10 \pm 2)\%$

[a] When calculating the atomic balances, it has to be taken into account that both tautomeric forms of TA contain two C atoms.

dering their observation impossible. As such, the assignment had to be made solely based on this band, making it a tentative one. A seemingly straightforward, alternative assumption could be that the 2378 cm^{-1} band is caused by the fully-hydrogenated form, H_3C–CH(–SH)–NH_2, however, the kinetic behavior of this band could not be explained by this species. Moreover, the computed vibrational frequencies of the ν[S–H] mode of this compound show no agreement with the experimental band position at all. It is also interesting to mention that the appearance of this band could also be observed upon the 216 nm laser photolysis or 5 keV electron bombardment of TA in *para*-H_2 matrix. The absorption band did not show up in Ar or when using longer wavelength UV photons, which suggest that H atoms forming upon the exposure to energetic radiation are responsible for the appearance of this band. However, the peak remained unassigned and therefore was not discussed by that study.[4]

3.5 Molar balance of the photolysis studies in *para*-H_2 matrices

The molar balances reflect well on what the kinetic plot in Figure 3 shows (Table 2). Right after the H-atom-generation process, the overall mixing ratio of thiols (along with a minor amount of NH_3) is equal to 4.0 ± 0.8 ppm, which corresponds to some 11-12% of the transformed TA thione tautomers (-37 ± 5 ppm). Nevertheless, this amount is still roughly an order of magnitude higher than when the tautomerization is achieved by laser UV or broadband Lyman-α irradiation; Ref. 4 found that less than 1% of the exposed thione precursor transformed into thiols at the end of the experiment. However, in that experiment, the thiols were also evidently subjected to UV-photodegradation (especially at shorter wavelengths) hence the seemingly less efficiency. The relative amount of H-atom-reaction products (excluding NH_3, whose mixing ratio quadruples) decreases somewhat overnight with regard to the thiones converted (5.3 ± 0.5 ppm to -66 ± 5 ppm, *i.e.*, approximately 8-10%); this points to the enhanced importance of alternative reaction pathways, *e.g.*, formation of (likely HCl) complexes when the system is left alone in the dark for an extended period of time.

The number of generated H atoms can be estimated indirectly from the integrated area of the HCl peak at 2895 cm^{-1} (they form in a 1 : 1 when the Cl atoms react with *para*-H_2 during the 2217 nm laser irradiation). The respective values are 788 and 985 ppm right after the H-atom generation and the next day, meaning that on average, roughly 200 H atoms are needed to produce one product molecule, which is in fair agreement with previous results.[5] This seemingly inefficient nature of the thione–thiol tautomerization (or H-atom reactions in general) induced by H atoms may be best explained by the occurrence of processes that work against the successful tautomerization, namely the recombination of H atoms into H_2 or when products or intermediates are efficiently converted back to the thione precursor. Such by-reactions may also yield an answer to the question of low product concentration with regard to that of the precursor after H atom generation. An alternative explanation would be the presence of more important reaction channels, such as the decomposition of the TA thione upon the exposure to H atoms. However, no small molecules or molecular fragments could be detected, which could be otherwise observed upon the destruction of TA by energetic irradiation.[4] Moreover, the theoretical results do not confirm this hypothesis. One should also assess the effect of the tentatively detected H_3C–Ċ(–SH)–NH_2 radical on the mixing ratios. As its mixing ratio could be estimated to be ≈ 10 and 30 ppm (by assuming an IR intensity of ≈ 100 km mol^{-1}) at the end of the H-atom generation and the end of the experiment, respectively, the atomic balances would increase to 39% and 55%, respectively, which agree better with the values obtained after UV photolysis of the same compound in the same matrix environment.[4]

4 Conclusions and Implications

Lapinski *et al.*[1] showed the possibility of thione–thiol tautomerization by exposing the matrix-isolated TA sample to energetic UV irradiation. Other examples are also known for such processes induced by UV photons, such as thiourea or N-methyl thiourea in various low-temperature matrices.[4,9,22–24] As such, radiation fields are well-known to facilitate tautomerization in general. However, the current study provides the first example for occurrence of the same tautomerization process without any irradiation, *i.e.*, simply in the presence of H atoms. Based on quantum-chemical considerations, a mechanism can also be provided. Namely, it is assumed to start with a barrierless H-atom addition on the S atom of the more stable thione tautomeric form. This process yields the radical, H_3C–Ċ(–SH)–NH_2, which connects the thione and thiol forms. The inert matrix environment allowed us to detect (even though only tentatively) this intermediate. Subsequently, a second H-atom reaction results in an H-atom abstraction and thus the formation of the more energetic thiol tautomers.

The present study undoubtedly shows that non-irradiation-induced thione–thiol tautomerization can occur in the presence of H atoms. Furthermore, its first and most important step is the H-atom addition on the S atom, implying that the latter element shows great H-atom acceptor capabilities. This holds even for a second H-atom addition leading to the eventual elimination of H_2S, which is also barrierless according to the computations.

View Article Online
DOI: 10.1039/D4CP02400A

However, H_2S is usually difficult to detect owing to its low IR absorption coefficients, hence this claim could not be supported experimentally. The process takes place in the dark, close to absolute zero temperature, in the lack of any radiation field, which may also imply astrochemical relevance as tautomerization could be a viable process in dense molecular clouds in the presence of H atoms. The results also point to a more general trend, namely, that the H-atom addition or abstraction may easily take place on the S atom or on the –SH group. This is in line with previous results with other sulfurous compounds and in contrast to what was found for the O-containing analogs.[5,25] In other words, this behavior seems to be ubiquitous for sulfur and it would be interesting to examine other related compounds in this regard, to better understand this phenomenon among S-bearing materials. Lastly, the existence of barrierless tautomerization upon exposure to H atoms should be studied in the case of molecules having other chalcogens as well, such as Se, to reveal how general this phenomenon is among the representatives of this group of the periodic system of elements.

Author Contributions

S. G.: Conceptualization, Formal analysis, Funding acquisition, Investigation, Methodology, Project administration, Supervision, Validation, Visualization, Writing – original draft. **B. K.**: Investigation, Writing – review & editing. **A. S.**: Investigation, Writing – review & editing. **G. T.**: Funding acquisition, Project administration, Resources, Supervision, Writing – review & editing.

Conflicts of interest

There are no conflicts to declare.

Data Availability Statement

Data for this article, including IR spectral files and Gaussian computational files are available at Zenodo.org at https://doi.org/10.5281/zenodo.12656866.

Acknowledgements

The authors thank the Hungarian Academy of Sciences for funding this research through the Lendület program. The Hungarian Scientific Research Fund (OTKA K143196) and the Institutional Excellence Program of the Eötvös Loránd University (TKP2020-IKA-05) are also acknowledged. S. G. was supported by the "Bolyai Ösztöndíj" of the Hungarian Academy of Sciences and by the "ÚNKP-23-5 New National Excellence Program" of the Ministry for Culture and Innovation from the source of the National Research, Development and Innovation Fund. B. K. and A. S. were both supported by the "ÚNKP-23-3 New National Excellence Program" of the Ministry for Culture and Innovation from the source of the National Research, Development and Innovation Fund. B. K. was also supported by the "DKOP-23 Doctoral Excellence Program" of the Ministry for Culture and Innovation from the source of the National Research, Development and Innovation Fund.

References

1 L. Lapinski, H. Rostkowska, A. Khvorostov and M. J. Nowak, *Physical Chemistry Chemical Physics*, 2003, **5**, 1524–1529.
2 S. Góbi, C. M. Nunes, I. Reva, G. Tarczay and R. Fausto, *Physical Chemistry Chemical Physics*, 2019, **21**, 17063–17071.
3 S. Góbi, I. Reva, I. P. Csonka, C. M. Nunes, G. Tarczay and R. Fausto, *Physical Chemistry Chemical Physics*, 2019, **21**, 24935–24949.
4 S. Góbi, B. Keresztes, A. Schneiker, G. Ragupathy and G. Tarczay, *Journal of Chemical Physics*, 2024, **160**, 024310.
5 B. Keresztes, S. Góbi and G. Tarczay, *Monthly Notices of the Royal Astronomical Society*, 2024, **527**, 12027–12043.
6 V. I. Feldman, *International Journal of Molecular Sciences*, 2023, **24**, 14510.
7 M. Tsuge and Y.-P. Lee, *Molecular and Laser Spectroscopy*, Elsevier, Amsterdam, Netherlands, 2020, ch. 5, pp. 167–215.
8 K. A. Haupa, P. R. Joshi and Y. Lee, *Journal of the Chinese Chemical Society*, 2022, **69**, 1159–1173.
9 S. Góbi, B. Keresztes, A. Schneiker and G. Tarczay, *Phys. Chem. Chem. Phys.*, 2024, **26**, 9963–9974.
10 S. Góbi, G. Ragupathy, G. Bazsó and G. Tarczay, *Photochem*, 2022, **2**, 563–579.
11 G. Bazsó, I. P. Csonka, S. Góbi and G. Tarczay, *Review of Scientific Instruments*, 2021, **92**, 124104.
12 P. L. Raston and D. T. Anderson, *Physical Chemistry Chemical Physics*, 2006, **8**, 3124–3129.
13 P. L. Raston and D. T. Anderson, *The Journal of Chemical Physics*, 2007, **126**, 021106.
14 S. C. Kettwich, P. L. Raston and D. T. Anderson, *The Journal of Physical Chemistry A*, 2009, **113**, 7621–7629.
15 P. L. Raston, S. C. Kettwich and D. T. Anderson, *Low Temperature Physics*, 2010, **36**, 392–399.
16 P. L. Raston, S. C. Kettwich and D. T. Anderson, *Journal of Molecular Spectroscopy*, 2015, **310**, 72–83.
17 M. J. Frisch, G. W. Trucks, H. B. Schlegel, G. E. Scuseria, M. A. Robb, J. R. Cheeseman, G. Scalmani, V. Barone, B. Mennucci, G. A. Petersson, H. Nakatsuji, M. Caricato, X. Li, H. P. Hratchian, A. F. Izmaylov, J. Bloino, G. Zheng, J. L. Sonnenberg, M. Hada, M. Ehara, K. Toyota, R. Fukuda, J. Hasegawa, M. Ishida, T. Nakajima, Y. Honda, O. Kitao, H. Nakai, T. Vreven, J. A. Montgomery Jr., J. E. Peralta, F. Ogliaro, M. Bearpark, J. J. Heyd, E. Brothers, K. N. Kudin, V. N. Staroverov, R. Kobayashi, J. Normand, K. Raghavachari, A. Rendell, J. C. Burant, S. S. Iyengar, J. Tomasi, M. Cossi, N. Rega, J. M. Millam, M. Klene, J. E. Knox, J. B. Cross, V. Bakken, C. Adamo, J. Jaramillo, R. Gomperts, R. E. Stratmann, O. Yazyev, A. J. Austin, R. Cammi, C. Pomelli, J. W. Ochterski, R. L. Martin, K. Morokuma, V. G. Zakrzewski, G. A. Voth, P. Salvador, J. J. Dannenberg, S. Dapprich, A. D. Daniels, Ö. Farkas, J. B. Foresman, J. V. Ortiz, J. Cioslowski and D. J. Fox, *Gaussian 09 Revision D.01*, 2013.
18 V. Barone, *The Journal of Chemical Physics*, 2004, **122**, 014108.
19 J. Bloino and V. Barone, *The Journal of Chemical Physics*, 2012, **136**, 124108.

View Article Online
DOI: 10.1039/D4CP02400A

20 M. Ruzi and D. T. Anderson, *The Journal of Physical Chemistry A*, 2013, **117**, 9712–9724.

21 T. Kobayashi, K. Seki, T. Tanaka and T. Takayanagi, *Computational and Theoretical Chemistry*, 2011, **963**, 256–262.

22 H. Rostkowska, L. Lapinski, A. Khvorostov and M. J. Nowak, *The Journal of Physical Chemistry A*, 2003, **107**, 6373–6380.

23 H. Rostkowska, L. Lapinski and M. J. Nowak, *Physical Chemistry Chemical Physics*, 2018, **20**, 13994–14002.

24 H. Rostkowska, L. Lapinski and M. J. Nowak, *Spectrochimica Acta Part A: Molecular and Biomolecular Spectroscopy*, 2024, 124139.

25 B. Keresztes, S. Góbi, I. P. Csonka, G. Ragupathy, G. Bazsó and G. Tarczay, *Monthly Notices of the Royal Astronomical Society*, 2023, **521**, 2649–2660.

View Article Online
DOI: 10.1039/D4CP02400A

Data Availability Statement

Data for this article, including IR spectral files and Gaussian computational files are available at Zenodo.org at https://doi.org/10.5281/zenodo.12656866.